Title
Method for producing identical spectral copies of ultra-broadband arbitrary light fields

Journal
Optics Express, 32(6)

ISSN
1094-4087

Authors
Chesnut, KD
Barty, CPJ

Publication Date
2024-03-11

DOI
10.1364/oe.516966

Research Article Vol. 32, No. 6 / 11 Mar 2024 / Optics Express 9790
Optics EXPRESS

Method for producing identical spectral copies of ultra-broadband arbitrary light fields

K. D. CHESNUT* AND C. P. J. BARTY

Department of Physics & Astronomy, University of California – Irvine, Reines Hall, Irvine, CA 92697, USA
*kyle.chesnut@uci.edu

Abstract: An ultra-broadband beam splitter arrangement, with a spectral amplitude response that is over seven orders-of-magnitude more uniform than broadband, multi-layer dielectric beam splitters, can be created by the combination of multiple Fresnel events on an uncoated, optical flat when used at a specific angle-of-incidence. This beam splitter arrangement produces three, spectral copies of the original, two of which have identical spectral phase. In this manuscript we derive the precise angle at which this maximally flat spectral amplitude response occurs for any material and present this angle's material and polarization dependence.

1. Introduction

The ability to create identical copies of a broadband optical source, whether coherent or low-coherence light, with a beam splitter is critical to many optical measurement applications such as Fourier transform spectroscopy [1] or any of the myriad of ultrafast pulse measurement techniques [2]. At large spectral widths, however, conventional metallic and multi-layer dielectric beam splitters exhibit high loss and/or large wavelength-dependent reflection and transmission. Currently, efficient ultra-broadband beam splitters are created using chirped multi-layer dielectric (MLD) coatings that also induce a phase response on the reflected pulse that is approximately equal to the phase response on the transmitted pulse due to material group delay dispersion (GDD) [3]. However, while the reflected and transmitted pulses are approximately similar, they are not identical. One method to ensure identical pulses is to have two MLD beam splitters and force each pulse copy to undergo one transmission and one reflection event [4]. While the two pulse copies produced in this way are identical, they are not exact replicas of the original input pulse unless the reflectivity or transmission does not vary as a function of frequency. Due to their discrete nature, MLD coatings also have a varying amplitude and dispersion response that is not easily described analytically. These variations, which are difficult to accurately quantify and compensate, are imparted onto the pulse copies distorting them from the original input pulse [5–7]. In this manuscript, we show that instead of using MLD coatings one can create an ultra-broadband beam splitter arrangement—with an exceptionally flat amplitude response within a Michelson interferometer setup—by orienting an uncoated optical flat at a precise angle-of-incidence (AOI), which we will call the Chesnut-Barty (CB) angle. At this angle, one can produce three, spectral copies of the original, two of which have identical spectral phase. In the following sections, the precise angle at which this maximally flat spectral amplitude response occurs for any material will be derived and the angle's material and polarization dependence will be presented.

2. Ultra-broadband Fresnel beam splitter arrangement

2.1. Configuration for minimal spectral amplitude distortion

When a light wave encounters the interface of two different dielectric media it is both reflected and refracted. For lossless media, the ratio at which the light wave's electric field is split into a

#516966 https://doi.org/10.1364/OE.516966
Journal © 2024 Received 27 Dec 2023; revised 19 Feb 2024; accepted 20 Feb 2024; published 4 Mar 2024

Optics EXPRESS

reflected and transmitted portion is described by the Fresnel equations [8],

$$R_s(\theta,\lambda) = \left\{ \frac{n_1(\lambda)cos(\theta) - n_2(\lambda)\sqrt{1 - \left[\frac{n_1(\lambda)}{n_2(\lambda)}sin(\theta)\right]^2}}{n_1(\lambda)cos(\theta) + n_2(\lambda)\sqrt{1 - \left[\frac{n_1(\lambda)}{n_2(\lambda)}sin(\theta)\right]^2}} \right\}^2 \tag{1}$$

$$T_s(\theta,\lambda) = 1 - R_s(\theta,\lambda) \tag{2}$$

$$R_p(\theta,\lambda) = \left\{ \frac{n_1(\lambda)\sqrt{1-\left[\frac{n_1(\lambda)}{n_2(\lambda)}sin(\theta)\right]^2} - n_2(\lambda)\cos(\theta)}{n_1(\lambda)\sqrt{1-\left[\frac{n_1(\lambda)}{n_2(\lambda)}sin(\theta)\right]^2} + n_2(\lambda)\cos(\theta)} \right\}^2 \tag{3}$$

$$T_p(\theta,\lambda) = 1 - R_p(\theta,\lambda). \tag{4}$$

Here, n_1 and n_2 are the index of refraction of air and the substrate respectively, θ is the AOI, λ is the wavelength, and R and T are the reflection and transmission intensity response, respectively, with subscript denoting the polarization. For simplicity, the polarization subscript will be omitted in the rest of the manuscript with the assumption that any process is purely in one linear polarization state. Figure 1(a), below, shows how a single input beam undergoes a Fresnel event each time it encounters the material interface, eventually splitting into multiple output beams.

In the simplest spectrally uniform beam splitter arrangement, the full beam is incident on an optical flat at some AOI where a portion of the beam is reflected, beam A in Fig. 1(a), and the remainder is transmitted into the optic. The transmitted portion of the beam transits the optical flat where it then undergoes a second transmission event at the back interface of the optic, beam B in Fig. 1(a). For the two beams to be identical they must have the exact same number of transmission and reflection events. Thus, as shown above in Fig. 1(b), the full Fresnel beam splitter arrangement consists of three identical uncoated optical flats. This allows the portion that was reflected off the first optical flat, beam A in Fig. 1(a), to be transmitted through an identical optical flat, while the portion that was first transmitted, beam B in Fig. 1(a), is then made to reflect off a third optical flat—both secondary events occur at the exact same AOI as the first. Now, each separate portion has undergone one Fresnel reflection (R) and two Fresnel transmissions (T) through the optical flat and experiences the same total amplitude response albeit in different orders—RTT and TTR. There is a third beam, beam C in Fig. 1(a), that naturally undergoes two transmissions and one reflection, in a TRT order, but has twice the material dispersion from transiting the optical flat twice. Using Eq. (2) or Eq. (4) above, the wavelength and angle dependence of the product of one Fresnel reflection and two Fresnel transmissions can be rewritten as R(1-R)(1-R) or,

$$A(\theta,\lambda) = R(\theta,\lambda)^3 - 2R(\theta,\lambda)^2 + R(\theta,\lambda). \tag{5}$$

To find the optimal reflection and transmission ratio that minimizes this function about a particular central wavelength, we take the derivative of Eq. (5) with respect to wavelength and set it equal to zero. The result is a simple quadratic relation, Eq. (7), with two roots, Eq. (8).

$$\frac{\partial A}{\partial \lambda} = \frac{\partial A}{\partial R}\frac{\partial R}{\partial n}\frac{dn}{d\lambda} = 0. \tag{6}$$

$$\frac{\partial A}{\partial \lambda} = 3R^2 - 4R + 1 = 0 \tag{7}$$

$$R = \frac{1}{3}, 1. \tag{8}$$

Optics EXPRESS

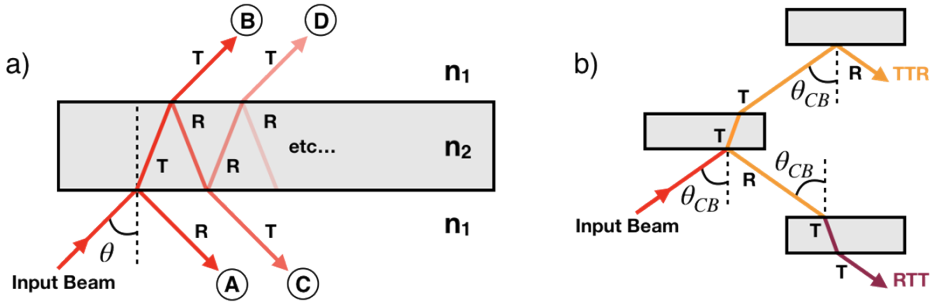

Fig. 1. a) Diagram of successive Fresnel transmission (T) and reflection (R) events on an uncoated optical flat from a single input beam. b) Schematic of an ultra-broadband, spectrally flat beam splitter arrangement composed of three identical uncoated optical flats.

The first root suggests that a maximally flat local spectral response occurs when the reflectivity is one-third and transmission is two-thirds, equating to 14.8% of the original pulse energy in each spectral copy, while the second root implies zero transmission and is thus of no practical interest. The reflectivity amplitude can be determined from either Eq. (1) or Eq. (3), depending on the polarization, which are only functions of the index of refraction, described by the Sellmeier equation, and the incident angle. Thus, the task for any specific center wavelength and material is to find the angle at which R, in Eq. (1) or Eq. (3), equals one-third.

The variation of spectral amplitude response as a function of angle is illustrated in Fig. 2 below, which shows the RTT amplitude response of an S-polarized pulse (a) and P-polarized pulse (b) centered at 800 nm incident on an optical flat of fused silica at various AOIs. The CB angle occurs at 72.95 degrees for S-polarized light and 82.25 degrees for P-polarized light.

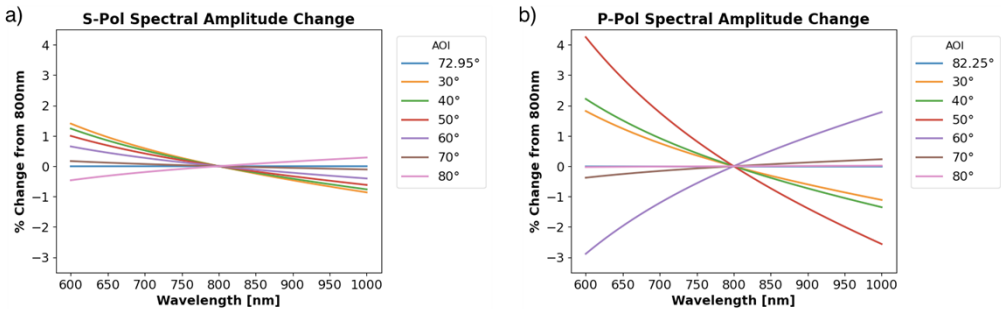

Fig. 2. Spectral amplitude variation centered at 800 nm, for the RTT response of a) S-polarized and b) P-polarized light incident on an optical flat, composed of fused silica, for various AOIs.

The spectral flatness of the RTT amplitude response of the fused silica optical flat with P-polarized light at the CB angle is significantly more uniform than a commercial MLD beam splitter, undergoing a RT response for a balanced interferometer [4], seen below in Fig. 3. Here, we quantify spectral amplitude flatness as the standard deviation of the relative difference of the spectral amplitude response from the center wavelength,

$$\sigma = \sqrt{\frac{\sum_{i=1}^{N}\left[\frac{A(\lambda_i)-A(\lambda_0)}{A(\lambda_0)}\right]^2}{N-1}}. \tag{9}$$

Optics EXPRESS

The spectral flatness standard deviations of the optical flat and the MLD beam splitter are 5.84E-8 and 1.60E-1 respectively, equating to over seven orders-of-magnitude increased flatness for the Fresnel beam splitter. Additionally, while each of the identical beam copies does experience material dispersion from the optical flat, the phase response is a smooth, quantifiable function that can be appropriately described by an analytical equation. In practice, one can compensate for the bulk of induced dispersion with an appropriate combination of prisms and/or gratings with the primary requirement of precise knowledge of residual dispersion terms—this is further expanded in a later section. In contrast, the dispersion ripples induced by an MLD coating cannot be fully compensated for [5–7].

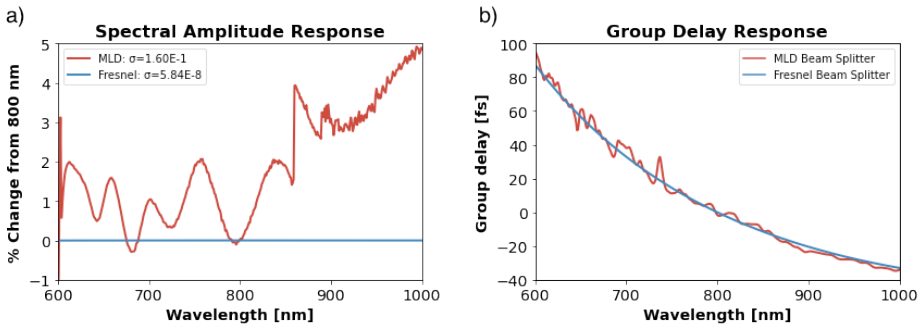

Fig. 3. a) Amplitude and b) group delay from the RTT response of a 6 mm thick fused silica, Fresnel beam splitter with P-polarized light at the CB angle versus the RT response of a commercial 50:50 MLD beam splitter (ThorLabs p/n UFBS5050) [9].

2.2. *Material and polarization dependencies*

While the first derivative of the total amplitude response as a function of wavelength at the CB angle, θ_{CB}, is zero, and thus the variation of the local spectral amplitude response is minimized, there is still some residual variation of the spectral amplitude response that is material and polarization dependent. The material- and polarization-dependent curvature can be quantified by examining the second derivative of the total amplitude response with respect to wavelength at the CB angle.

$$\left(\frac{\partial^2 A}{\partial \lambda^2}\right)_{\theta} = \frac{\partial^2 A}{\partial \lambda \partial R}\frac{\partial R}{\partial n}\frac{dn}{d\lambda} + \frac{\partial A}{\partial R}\frac{\partial^2 R}{\partial \lambda \partial n}\frac{dn}{d\lambda} + \frac{\partial A}{\partial R}\frac{\partial R}{\partial n}\frac{d^2 n}{d\lambda^2} \tag{10}$$

At the CB angle the partial derivative of the amplitude with respect to Fresnel reflection is zero, as shown in Eq. (6) and Eq. (7), canceling the last two terms in Eq. (1)0. From Eq. (7) we find,

$$\frac{\partial^2 A}{\partial \lambda \partial R} = (6R - 4)\frac{\partial R}{\partial n}\frac{dn}{d\lambda}. \tag{11}$$

Substituting Eq. (1)1 into Eq. (10) and noting that at the CB angle the Fresnel reflection amplitude, R, is one-third we find,

$$\left(\frac{\partial^2 A}{\partial \lambda^2}\right)_{\theta_{CB}} = \frac{\partial^2 A}{\partial \lambda \partial R}\frac{\partial R}{\partial n}\frac{dn}{d\lambda} = -2\left(\frac{\partial R}{\partial n}\right)^2\left(\frac{dn}{d\lambda}\right)^2. \tag{12}$$

Thus, we see that the curvature is a result of the change in Fresnel reflection amplitude due to a change of index of refraction and the change in index of refraction due to a change of wavelength.

Focusing first on the derivative of the index of refraction with respect to wavelength, also called the chromatic dispersion, less dispersive materials (i.e., materials with at flatter index of

Optics EXPRESS

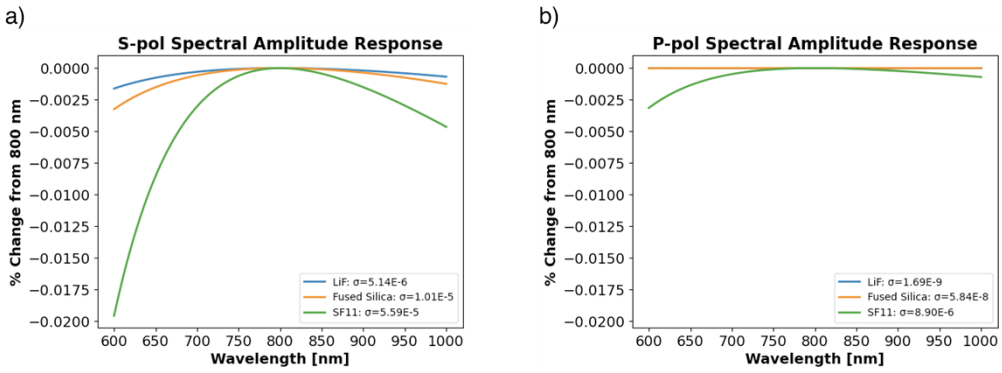

Fig. 4. Spectral amplitude variation, centered at 800 nm, for three different materials each at their CB angle-of-incidence for a) S-polarized light and b) P-polarized light.

refraction curve) will produce less amplitude variation across the spectrum of interest. Most optical materials have an absorption peak in the UV range, and as the spectrum approaches this peak the slope of the index of refraction curve increases. Thus, optical materials with absorption peaks further from the spectral range of interest will produce a flatter total amplitude response. Additionally, increasing the index of refraction reduces the CB angle; this effect is much more prominent for S-polarized light. At 800 nm, lithium fluoride has an index of refraction of 1.3890, fused silica of 1.4533, and SF11 of 1.7648, giving balanced amplitude angles of 74.46 degrees, 72.95 degrees, and 66.16 degrees respectively for S-polarized light [10]. Comparing these three different materials, above in Fig. 4, shows the significant difference in total amplitude response across 600 nm to 1000 nm. In the S-polarized case, LiF has a spectral amplitude standard deviation of 5.14E-6, fused silica of 1.01E-5, and SF11 of 5.59E-5. For P-polarization, the CB angles are 82.23 degrees, 82.25 degrees, and 82.78 degrees for LiF, fused silica, and SF11 respectively. Here, LiF has a spectral amplitude standard deviation of 1.69E-9, fused silica of 5.84E-8, and SF11 of 8.90E-6. The increased amplitude variance corresponds to the increased

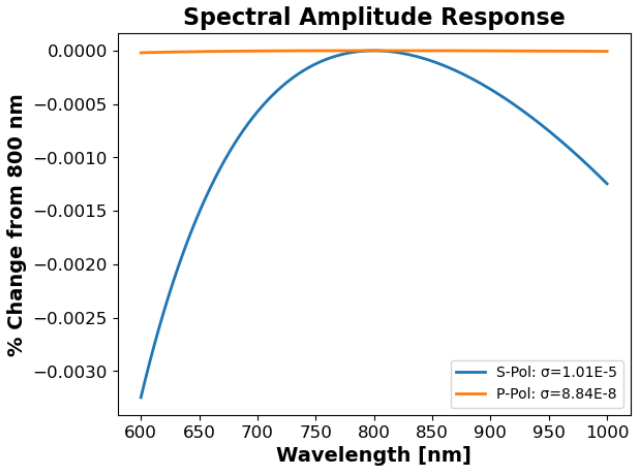

Fig. 5. Spectral amplitude response of S-polarized and P-polarized light, centered at 800 nm, for fused silica Fresnel beam splitter set at their respective CB angles of 72.95 degrees and 82.25 degrees.

Optics EXPRESS

chromatic dispersion at 800 nm, with a chromatic dispersion of 1.09E-2 um^{-1} for LiF, −1.73E-2 um^{-1} for fused silica, and −5.77E-2 um^{-1} for SF11 [10].

As stated above, the spectral amplitude response also depends on the polarization of the incident light due to the difference in the Fresnel reflection equations for S and P-polarized light. The CB angle of S-polarized light has a much greater sensitivity to the material index of refraction than P-polarized light, allowing one to effectively tune the CB AOI by selecting a different optical material. However, S-polarized light has an increased spectral amplitude variation compared to P-polarized light, shown above in Fig. 5, with all else equal. This can be understood by examining the derivative of the Fresnel reflection responses, Eq. (1) and Eq. (3), with respect to the index of refraction. The functional form is complicated and not elucidating; however, evaluating the derivative at the index of refraction value for 800 nm light, and at the CB angle, in fused silica results in a value of −0.0348 for P-polarized light and 0.4669 for S-polarized light. The lower magnitude value for P-polarized light explains the lower spectral amplitude variation, compared to S-polarized light.

3. Interferometer with near uniform spectral response

3.1. Michelson interferometer design

The Fresnel beam splitter arrangement, shown above in Fig. 1(b), can be simplified to a single optical flat by incorporating retroreflectors in each of the two beam paths as seen below in Fig. 6. In doing so, one eliminates the primary error sources of optical flat thickness mismatch and AOI discrepancy between the primary and secondary Fresnel events. Furthermore, by varying the offset of the two paths one can configure the setup to act as either a beam splitter or Michelson interferometer.

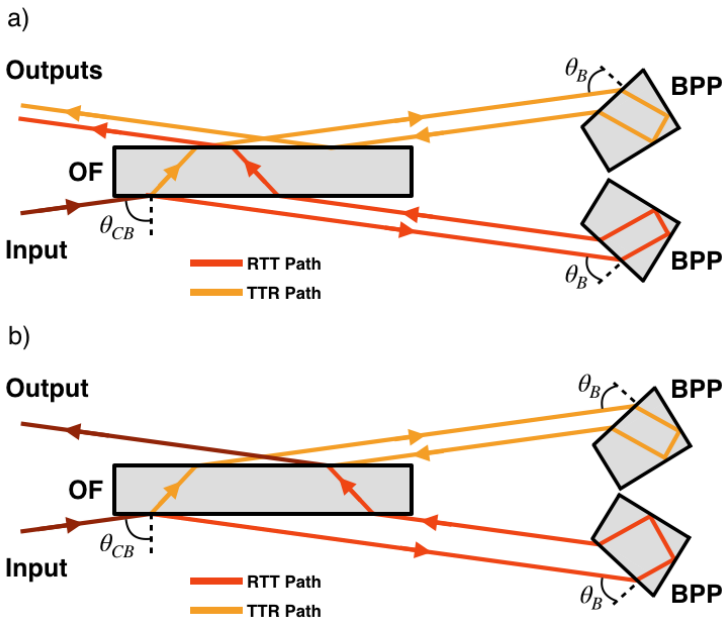

Fig. 6. Fresnel beam splitter arrangement using a single optical flat (OF) and two Brewster's angle Porro prisms (BPP) operating in a) beam splitter and b) Michelson interferometer configurations.

To maintain the overall system spectral amplitude flatness, the retroreflectors should be total internal reflection (TIR) prisms as opposed to mirrors. TIR retroreflectors maintain the same

Optics EXPRESS

material path length while varying the return beam offset allowing the two beam paths to preserve equal dispersion, insofar as the two TIR retroreflectors are identical. In the p-polarization case, this can be accomplished using a Brewster's angle Porro prism (BPP)—a Pellin-Broca prism operated as a retroreflector with the incident light at Brewster's angle [11]. Here, the TIR retroreflectors induce only a Fresnel transmission response at Brewster's angle on each beam's spectral amplitude distribution as shown below in Fig. 7. The spectral flatness standard deviation of the Brewster's angle transmission is 2.27E-7, over a spectral range of 600-1000 nm, compared to the Fresnel beam splitter's of 5.84E-8 over the same spectral region. While this decreases the spectral amplitude flatness it is still over six orders of magnitude better than the commercial MLD beam splitter.

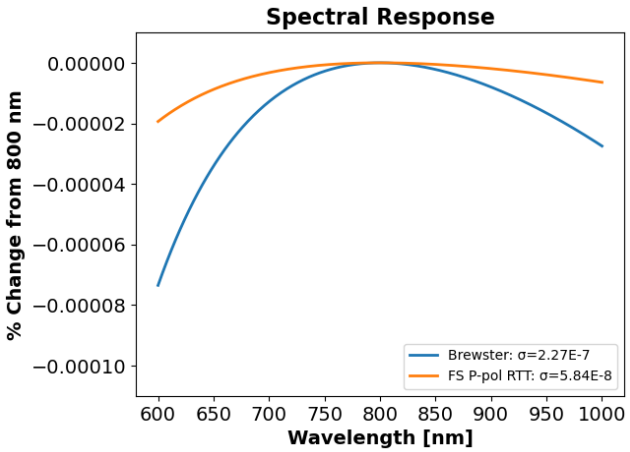

Fig. 7. Spectral amplitude response of Brewster's angle transmission for 800 nm light through fused silica compared to the P-polarized RTT response of fused silica at the CB angle.

While the above has been for the simplest case of one reflection and two transmission events, this scheme can be extended to produce an increased number of identical pulses by including more Fresnel events. The next iteration produces fives copies of the beam by the following permutations: TTRR, RTTR, RTRT, TRTR, and RRTT. Following the same procedure as before, the flattest amplitude distribution is given when the Fresnel reflection response is set to one-half the incident beam energy with each of the identical beam copy containing 6.25% of the original energy. In addition to lower energy per beam copy, the higher-level permutations require, in practice, a more complicated optical setup and a larger optical flat as the beam splitter. In 2019, a variation of this beam splitter concept was employed to achieve achromatic nulling in a Mach-Zender interferometer for absorption spectroscopy measurements [12]. This study used a combination of RTTTT and TTTRT Fresnel events at an angle near that for maximum efficiency, which happens to correspond to flattest spectral amplitude response as well. However, it required three separate uncoated optical flats in the experimental setup introducing an undesirable error source due to the variation in thickness. In contrast, the Michelson interferometer using the RTT and TTR Fresnel events, shown above in Fig. 6, is relatively simple and requires only a single uncoated optical flat beam splitter and two Brewster Porro prisms.

3.2. *Residual pulse distortions*

The Fresnel beam splitter arrangement produces two identical pulses that are near exact spectral copies of the input pulse with a known—to the accuracy of the measured physical dimensions of the optics—and fixed temporal distortion that in principle can be measured. For Fourier

Optics EXPRESS

transform spectroscopy applications the dispersion of the system does not matter; however, it is a concern when using this design for several interferometric ultrafast pulse measurement applications [13–15]. The fundamental necessity here is not the complete compensation of all higher-order dispersion terms induced by the beam splitter arrangement, but the compensation of the bulk dispersion and precise knowledge of the residual higher-order terms to be numerically backed out of the pulse measurement output. With the Fresnel beam splitter arrangement this task is relatively simple as the material dispersion of the system can be analytically described and accurately measured. In contrast, this is more difficult when using MLD coated optics due to the variable, non-analytic dispersion response and variation between coating runs.

Consider the Fresnel beam splitter arrangement shown in Fig. 6. using an optical flat composed of fused silica and a 1 mm diameter, p-polarized input beam with spectrum centered at 800 nm. Here, the CB angle is 82.25 degrees. To separate the RTT beam from the TRT beam by two beam diameters requires the optical flat of at least 8 mm thickness. This thickness can be reduced, at the expense of added complexity, by including a spatial filter post-recombination to filter out the unwanted secondary beams [12]. The beam path in the BPPs is determined by construction; here we will consider typical values of an off-the-shelf model [16], but this can be further optimized. With a beam path in the fused silica BPPs of approximately 30 mm the total material path length for each beam copy is 40.9 mm equating to a GDD of 1479 fs^2 and a TOD of 1126 fs^3. These values are constant for any pulse measurement and can either be deconvolved from the measurement of pulses using the existing interferometer, or approximately compensated with Brewster prism pairs. For example, 1479 fs^2 of GDD can be completely compensated using a double pass two prism compressor composed of fused silica Brewster prisms separated by 777 mm with 1 mm of insertion on the first prism and 2 mm of insertion on the second prism. This would result in a pulse with a residual TOD of -636 fs^3.

Angular dispersion, in both the optical flat and BPP, will generate a spatial chirp on each of the two split pulses. The magnitude of the spatial chirp is dependent on material selection, dimensions of the optics, CB angle, center wavelength of pulse, and beam diameter. With the optics oriented as drawn in Fig. 6, the direction of the spatial chirp is reversed in the BPP compared to the OF. In principle, this setup can be designed so the spatial chirp in the two optics nearly cancel each other. Using the same physical arrangement as the temporal dispersion discussion, 600 nm light will be shifted by 37.3 µm from the center wavelength, a spatial chirp rate of ~0.19 µm/nm, while the 1000 nm light is shifted 24.7 µm, a spatial chirp rate of ~0.12 µm/nm, with a majority of the spatial chirp coming from the BPP. This is well below the 1 µm/nm spatial chirp accuracy of a GENOUILLE pulse measurement system [17]. For a 1 mm diameter beam this results in an ellipticity of ~94%. The spatial chirp is negligible for any interferometric application utilizing a single photodiode as the detector. As with the temporal dispersion, the spatial chirp is known to the accuracy of the physical dimensions of the optics used and can be numerically included in any pulse characterization algorithm.

4. Conclusion

An ultra-broadband beam splitter arrangement, with spectral amplitude flatness over seven orders-of-magnitude more uniform than commercial MLD beam splitters, can be created by combining one Fresnel reflection and two Fresnel transmission events from an uncoated optical flat at the CB angle—the angle at which the one Fresnel reflection is one-third of the input beam energy—to produce three near identical pulse copies. Material selection of the optical flat and polarization state of the incoming beam are the primary variables that affect the spectral amplitude flatness and the AOI of the CB angle. While P-polarized light results in a flatter spectral response, S-polarized light allows for a greater amount of CB AOI tuning through material index of refraction selection. Here, the CB angle is inversely proportional to the material index of refraction and lower chromatic dispersion in the material results in a flatter spectral

Optics EXPRESS

amplitude response for both polarization states. While methods to create two identical pulse pairs have existed [4], to date there has not been a way to create identical copies of the original ultra-broadband pulse.

This near-zero spectral distortion, ultra-broadband beam splitter arrangement enhances the accuracy of any Michelson interferometer optical measurement technique where the input source is also the signal to be measured. This pertains to Fourier transform spectroscopy applications such as, but not limited to, astronomical spectroscopy [18] and atmospheric sensing [19]. For example, in stellar spectroscopy the depth of absorption line features are the primary input variables to numerical simulations that determine star temperature, chemical abundance, and atmospheric parameters; a comparative study of different codes found the absorption line depth error greater than 5% to produce unreliable results [20]. Modification to the measured spectrum will shift the relative ratio of absorption lines, as well as the absolute position of the absorption peaks and line width. This beam splitter arrangement has even greater benefit for ultrafast pulse measurement systems where knowledge of both the spectral amplitude and phase is important. Most ultrafast pulse measurement systems are essentially phase-retrieval schemes that, when combined with the spectral amplitude, allow one to calculate the profile of the temporal electric field [13–15]. If the pulse measurement system distorts the phase of the pulse it is measuring an incorrect temporal pulse profile and width will be output. This is critical for applications utilizing ultrashort pulse lasers that are sensitive to the pulse duration [21], temporal profile [22], and pulse chirp [23].

Disclosures. The authors declare no conflicts of interest.

Data availability. Data underlying the results presented in this paper are not publicly available at this time but may be obtained from the authors upon reasonable request.

References

1. R. J. Bell, *Introductory Fourier Transform Spectroscopy*, Academic Press Inc., New York, NY, USA (1972).
2. R. Trebino, R. Jafari, S. A. Akturk, *et al.*, "Highly reliable measurement of ultrashort laser pulses," J. Appl. Phys. **128**(17), 171103 (2020).
3. J. Kim, J. R. Birge, V. Sharma, *et al.*, "Ultrabroadband beam splitter with matched group-delay dispersion," Opt. Lett. **30**(12), 1569–1571 (2005).
4. C. P. J. Barty, B. E. Lemoff, and C. L. Gordon III, "Generation, measurement, and amplification of 20-fs high-peak-power pulses from a regeneratively initiated, self-mode-locked Ti:sapphire laser," *Proc. SPIE 1861 Ultrafast Pulse Generation and Spectroscopy*, (1993).
5. G. Steinmeyer, "Disersion Oscillations in Ultrafast Phase-Correction Devices," IEEE J. Quantum Electron. **39**(8), 1027–1034 (2003).
6. G. Steinmeyer, "Femtosecond dispersion compensation with multilayer coatings: toward the optical octave," Appl. Opt. **45**(7), 1484–1490 (2006).
7. T. A. Laurence, D. A. Alessi, E. Feigenbaum, *et al.*, "Mirrors for petawatt lasers: Design principles, limitations, and solutions," J. Appl. Phys. **128**(7), 071101 (2020).
8. E. Hecht, *Optics* 5th Edition, p100, *Pearson Publishing Inc.*, New York, NY (2015).
9. ThorLabs, "Ultrafast Beamsplitter UFB5050 Raw Data," (2023), https://www.thorlabs.com/images/tabimages/UFB505002_data.xlsx.
10. M. N. Polyanskiy, "Refractive index database,' (2023), https://refractiveindex.info.
11. H. Moosmüller, "Brewster's Angle Porro Prism: A Different Use for a Pellin-Broca Prism," Appl. Opt. **37**(34), 8140–8141 (1998).
12. T. Buberl, P. Sulzer, A. Leitenstorfer, *et al.*, "Broadband interferometric subtraction of optical fields," Opt. Express **27**(3), 2432–2443 (2019).
13. J.-C. M. Diels, "Control and measurement of ultrashort pulse shapes (in amplitude and phase) with femtosecond accuracy," Appl. Opt. **24**(9), 1270 (1985).
14. D. J. Kane and R. Trebino, "Characterization of Arbitrary Femtosecond Pulses Using Frequency-Resolved Optical Gating," IEEE J. Quantum Electron. **29**(2), 571–579 (1993).
15. C. Iaconis and I. A. Walmsley, "Spectral phase interferometry for direct electric-field reconstruction of ultrashort optical pulses," Opt. Lett. **23**(10), 792–794 (1998).
16. ThorLabs, "ADBU-10 – Pellin Broca Prism, 10 mm Square Aperture, UV Fused Silica," (2024), https://www.thorlabs.com/thorproduct.cfm?partnumber=ADBU-10.
17. Swamp Optics, "Near-IR GENOUILLEs," (2020), https://www.swampoptics.com/assest/brochure-near-ir-genouilles-2020-01.pdf.

Optics EXPRESS

18. S. T. Ridgway and J. W. Brault, "Astronomical Fourier Transform Spectroscopy Revisited," Annu. Rev. Astron. Astrophys. **22**(1), 291–317 (1984).
19. Z. Bacsik, J. Mink, and G. Keresztury, "FTIR Spectroscopy of the Atmosphere. I. Principles and Methods," Appl. Spectrosc. Rev. **39**(3), 295–363 (2004).
20. S. Blanco-Cuaresma, "Modern stellar spectroscopy caveats," MNRAS **486**(2), 2075–2101 (2019).
21. A. Das, A. Wang, O. Uteza, *et al.*, "Pulse-duration dependence of laser-induced modifications inside silicon," Opt. Express **28**(18), 26623–26635 (2020).
22. M. D. Perry, T. Ditmire, and B. C. Stuart, "Self-phase modulation in chirped-pulse amplification," Opt. Lett. **19**(24), 2149–2152 (1994).
23. A. Jain and D. N. Dupta, "Optimization of electron bunch quality using a chirped laser pulse in laser wakefield acceleration," Phys. Rev. Accel. Beams **24**(11), 111302 (2021).